research papers

Structure of human PNP complexed with ligands

**Fernanda Canduri,[a,b]
Rafael Guimarães Silva,[c]
Denis Marangoni dos Santos,[a]
Mário Sérgio Palma,[b,d]
Luiz Augusto Basso,[c]
Diógenes Santiago Santos[c,e]* and
Walter Filgueira de Azevedo
Jr[a,b]***

[a]Programa de Pós-Graduação em Biofísica Molecular, Departamento de Física, UNESP, São José do Rio Preto, SP 15054-000, Brazil, [b]Center for Applied Toxicology, Instituto Butantan, São Paulo, SP 05503-900, Brazil, [c]Rede Brasileira de Pesquisas em Tuberculose, Departamento de Biologia Molecular e Biotecnologia, UFRGS, Porto Alegre, RS 91501-970, Brazil, [d]Laboratory of Structural Biology and Zoochemistry–CEIS/Department of Biology Institute of Biosciences, UNESP, Rio Claro, SP 13506-900, Brazil, and [e]Centro de Pesquisas em Biologia Molecular e Funcional/ PUCRS, Avenida Ipiranga 6681, Tecnopuc, Partenon, 90619-900, Porto Alegre, RS, Brazil

Correspondence e-mail: diogenes@pucrs.br, walterfa@ibilce.unesp.br

Purine nucleoside phosphorylase (PNP) is a key enzyme in the purine-salvage pathway, which allows cells to utilize preformed bases and nucleosides in order to synthesize nucleotides. PNP is specific for purine nucleosides in the β-configuration and exhibits a strong preference for purines containing a 6-keto group and ribosyl-containing nucleosides relative to the corresponding analogues. PNP was crystallized in complex with ligands and data collection was performed using synchrotron radiation. This work reports the structure of human PNP in complex with guanosine (at 2.80 Å resolution), 3′-deoxyguanosine (at 2.86 Å resolution) and 8-azaguanine (at 2.85 Å resolution). These structures were compared with the PNP–guanine, PNP–inosine and PNP–immucillin-H complexes solved previously.

1. Introduction

Mammalian purine nucleoside phosphorylase (PNP) catalyses the phosphorolysis of the natural 6-oxypurine (deoxy)-nucleosides of guanine, hypoxanthine and a number of related nucleoside compounds and are inactive against (deoxy)-adenosine or the pyrimidine (deoxy)nucleosides (Kim *et al.*, 1968). The catalytic efficiency is high for the deoxyguanosine nucleoside that characterizes its biological function (Stoeckler *et al.*, 1980). PNP is present at micromolar concentrations in blood cells and is coupled to a substrate-trapping phenomenon known as catalytic commitment (Northrop, 1975; Kline & Schramm, 1993; Schramm, 2002).

The (deoxy)nucleoside substrates of PNP are normally absent from the blood as a result of robust PNP catalytic activity in the intestine, liver, erythrocytes, lymphocytes, spleen and kidney (Simmonds *et al.*, 1987; Cohen *et al.*, 1976). The activity of PNP in the blood alone causes injected nucleoside substrates to undergo phosphorolysis with a half-life of a few seconds. However, PNP substrates accumulate in the blood and urine of PNP-deficient patients, replacing uric acid, which is dramatically reduced in both blood and urine (Hershfield & Mitchell, 2001). The pathway of purine-nucleoside degradation requires PNP and without it nucleo-sides accumulate, purine bases for salvage pathways and degradation are depleted and the rate of *de novo* purine synthesis increases (Cohen *et al.*, 1976; Ealick *et al.*, 1990). Overproduction of purines is not accompanied by purine-precipitation disorders in PNP deficiency since the (deoxy)-nucleosides are more soluble than uric acid. Blood levels of these metabolites are significant and the primary purine-excretion products are urinary nucleosides. In addition, (deoxy)nucleoside salvage increases because of excess substrate availability. Infants with a rare T-cell immuno-

Table 1
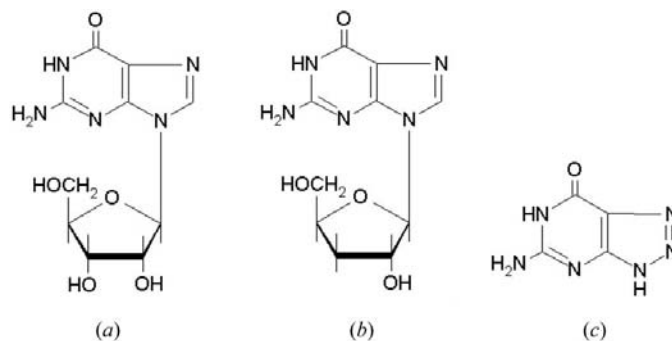Data-collection and refinement statistics.

Values in parentheses are for the highest resolution shell.

	PNP–Guo	PNP–dGuo	PNP–azaGua
Unit-cell parameters			
$a = b$ (Å)	139.38	141.32	139.28
c (Å)	160.40	162.62	161.42
$\alpha = \beta$ (°)	90.00	90.00	90.00
γ (°)	120.00	120.00	120.00
Space group	$R32$	$R32$	$R32$
No. of measurements with $I > 2\sigma(I)$	78490	57008	32698
No. of independent reflections	14265	13192	12763
Resolution range used in refinement (Å)	8.0–2.80	8.0–2.86	7.0–2.85
Highest resolution shell (Å)	2.95–2.80	3.01–2.86	3.01–2.85
Overall completeness (%)	95.8 (97.6)	91.0 (93.7)	91.0 (90.4)
R_{sym}† (%)	5.8 (26.8)	5.7 (25.1)	9.9 (19.3)
R factor‡ (%)	20.6	18.0	18.6
R_{free}§ (%)	26.7	24.9	26.3
B values¶ (Å²)			
Main chain	31.38	38.48	26.27
Side chains	34.96	42.69	29.95
Ligand	41.73	36.30	45.94
Waters	21.25	39.96	29.07
Sulfate groups	39.74	58.95	42.35
Observed r.m.s.d. from ideal geometry			
Bond lengths (Å)	0.018	0.015	0.013
Bond angles (°)	2.01	1.92	1.90
Dihedrals (°)	25.21	25.45	25.69
Ramachandran plot, residues in			
Most favoured regions (%)	79.9	82.0	79.9
Additionally allowed regions (%)	16.8	14.8	13.9
Generously allowed regions (%)	1.6	1.6	4.5
Disallowed regions (%)	1.6	1.6	1.6
No. of water molecules	17	30	19
No. of sulfate groups	3	3	4

† $R_{sym} = 100\sum |I(h) - \langle I(h)\rangle|/\sum I(h)$, where $I(h)$ is an observed intensity and $\langle I(h)\rangle$ is the mean intensity of reflection h over all measurements of $I(h)$. ‡ R factor = $100\sum |F_{obs} - F_{calc}|/\sum F_{obs}$, the sums being taken over all reflections with a $F/\sigma(F) > 2$ cutoff. § R_{free} is the R factor for 10% of the data which were not included during crystallographic refinement. ¶ Average B values for all non-H atoms.

Figure 1
Molecular structures of PNP substrates. (*a*) Guanosine, (*b*) 3'-deoxyguanosine, (*c*) 8-azaguanine.

deficiency lacking PNP show altered pathways of purine metabolism. Deoxyguanosine accumulates in the blood as a result of PNP deficiency and is transported and phosphorylated by T-cell deoxynucleoside kinases to form pathologically elevated levels of dGTP specifically in these cells (Krenitsky *et al.*, 1976; Ullman *et al.*, 1979). Inhibition of PNP was soon identified as a target for the regulation of undesirable T-cell proliferation and a campaign was launched for the discovery of powerful inhibitors (Ealick *et al.*, 1991). The catalytic mechanism of PNP has been extensively studied by enzyme kinetics (Erion *et al.*, 1997). PNP is specific for purine nucleosides in the β-configuration and cleaves the glycosidic bond with inversion of configuration to produce α-ribose 1-phosphate. Bond breaking is far ahead of bond making in the phosphorolytic direction and the transition state has considerable oxocarbenium-ion character. Further evidence for a transition state with an oxocarbenium ion is apparent from kinetic isotope studies on the PNP-catalyzed hydrolysis and methanolysis of inosine (Kline & Schramm, 1995). Kinetic studies have also provided some insight into the identity of the active-site residues that participate in catalysis (Erion *et al.*, 1997). Knowledge of enzymatic transition states permits the

logical design of transition-state analogues. Immucillin-H, a powerful transition-state inhibitor for human PNP, has entered clinical trials as an anti-T-cell agent (Schramm, 2003; de Azevedo *et al.*, 2003b). In the presence of deoxyguanosine, this molecule inhibits the proliferation of activated human lymphocytes. This inhibition is associated with an intracellular elevation of dGTP in the cells (Bantia *et al.*, 2001, 2003). Narayana *et al.* (1997) solved the structure of human PNP complexed with guanine at 2.75 Å and de Azevedo, Canduri *et al.* (2003) solved the structure of the apoenzyme at 2.3 Å resolution. The crystal structures of the complexes between immucillin-H, acyclovir and other ligands with PNP clearly showed the importance of the residues Asn243 and Glu201 for ligand specificity (Ealick *et al.*, 1991; Canduri *et al.*, 2004; Canduri, Fadel, Dias *et al.*, 2005; Canduri, Fadel, Basso *et al.*, 2005).

Here, we describe the crystallographic structures of the complexes HsPNP–guanosine (HsPNP–Guo), HsPNP–3'-deoxyguanosine (HsPNP–dGuo) and HsPNP–8-azaguanine (HsPNP–azaGua). Fig. 1 shows the molecular structures of 3'-deoxyguanosine, guanosine and 8-azaguanine. The previously solved complex structures of PNP–guanine (PNP–Gua; de Azevedo *et al.*, 2003a), PNP–inosine (PNP–Ino; Canduri *et al.*, 2004) and PNP–immucillin-H (PNP–ImmH; de Azevedo *et al.*, 2003b) were used to compare the modes of binding to the active site.

2. Materials and methods

2.1. Crystallization and data collection

Recombinant human PNP (HsPNP) was expressed and purified as described previously (Silva *et al.*, 2003). HsPNP was crystallized using the experimental conditions described elsewhere (Cook *et al.*, 1981) and the best crystals were obtained after 2 d. In brief, a PNP solution was concentrated to 12 mg ml^{-1} in 10 m*M* potassium phosphate buffer pH 7.1 and incubated in the presence of 0.6 m*M* ligand (Sigma Co.). Hanging drops were equilibrated by vapour diffusion at 298 K against reservoir containing 21% saturated ammonium sulfate solution in 0.05 *M* citrate buffer pH 5.3.

In order to increase the resolution of the crystals of the PNP complexes, we collected data from a flash-cooled crystal at 104 K. Prior to flash-cooling, glycerol was added to the crystallization drop up to 50%(*v*/*v*). X-ray diffraction data were collected at a wavelength of 1.431 Å using the Synchrotron Radiation Source (Station PCr, Laboratório Nacional de Luz Síncrotron, LNLS, Campinas, Brazil) and a CCD detector (MAR CCD). X-ray diffraction data were processed to 2.80, 2.86 and 2.85 Å resolution for PNP–guanosine, PNP–3′-deoxyguanosine and PNP–8-azaguanine, respectively. The crystallographic data were processed using the program *MOSFLM* (Collaborative Computational Project, Number 4, 1994) and scaled with the program *SCALA* (Collaborative Computational Project, Number 4, 1994).

The complexes crystallized in the trigonal space group *R*32 and the volume of the unit cell is 2.81×10^6 Å^3, compatible with one monomer in the asymmetric unit with a V_M value of 4.88 Å^3 Da^{-1}. Assuming a value of 0.74 cm^3 g^{-1} for the protein partial specific volume, the calculated solvent content in the crystal is 75.0% and the calculated crystal density is 1.04 g cm^{-3}. The X-ray diffraction statistics are summarized in Table 1.

2.2. Crystal structure

The crystal structures of the complexes were determined by standard molecular-replacement methods using the program *AMoRe* (Navaza, 1994), as incorporated in the *CCP*4 program package (Collaborative Computational Project, Number 4, 1994), using as search model the structure of human PNP in complex with acyclovir (PDB code 1pwy; dos Santos *et al.*, 2003) to solve the PNP–Guo and PNP–dGuo complexes and the structure of PNP in complex with guanine (PDB code 1v2h; de Azevedo *et al.*, 2003a) to solve the PNP–azaGua complex. The ligands and water molecules were removed from the search models. The resolution range used in molecular replacement was 8.0–3.5 Å. Structure refinement was performed using *X-PLOR* (Brünger, 1992).
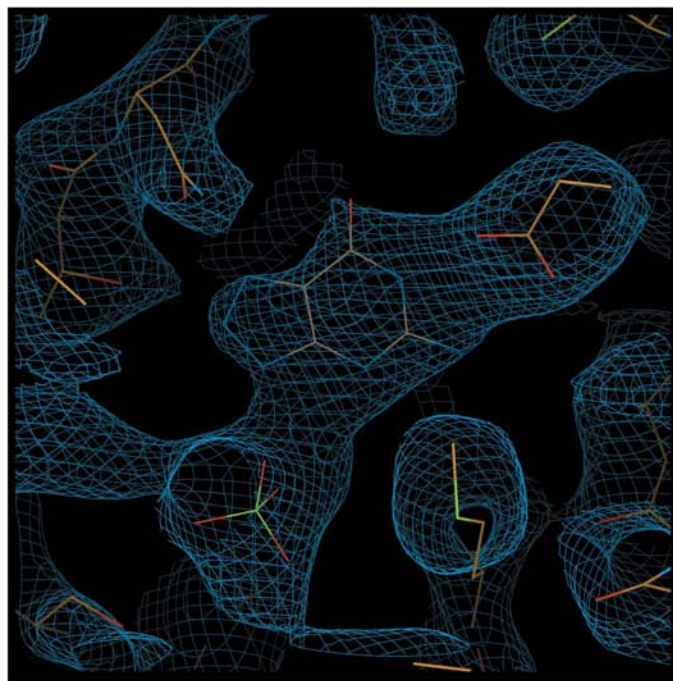
Further refinement in *X-PLOR* continued with simulated annealing using the slow-cooling protocol followed by alter-
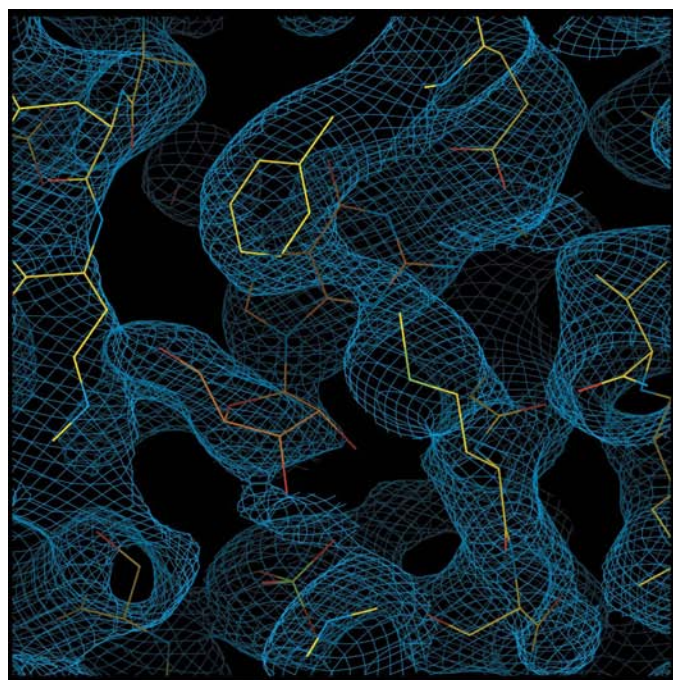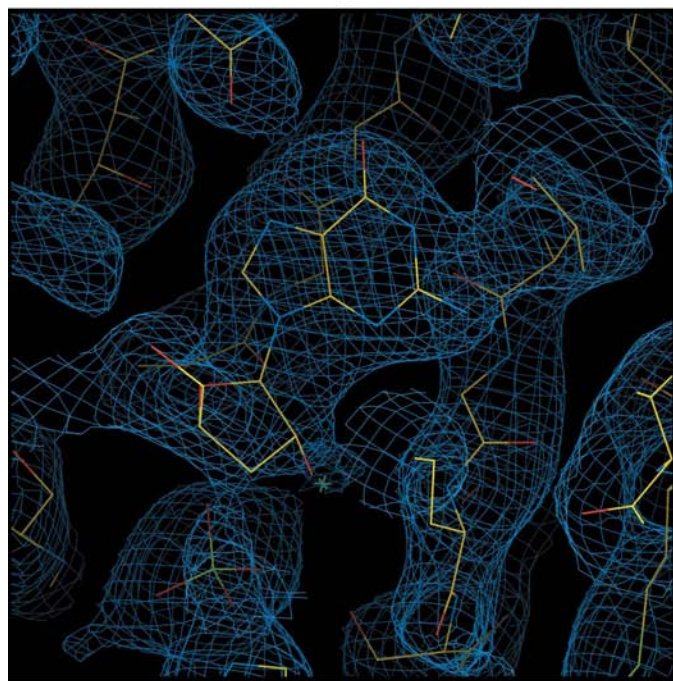
Figure 2
Electron-density map ($2F_{obs} - F_{calc}$, 1σ cutoff) for the active-site regions of (*a*) HsPNP–guanosine, (*b*) HsPNP–3′-deoxyguanosine and (*c*) HsPNP–8-azaguanine.

nating cycles of positional refinement and manual rebuilding using *XtalView* (McRee, 1999). Reflections with $I > 2\sigma(I)$ were used in the refinement. Initial models of the ligands were generated using *SYBYL* (Tripos Co.). Finally, the positions of the ligands, water and sulfate molecules were checked and corrected in $F_{obs} - F_{calc}$ maps.

Root-mean-square deviation differences from ideal geometries for bond lengths, angles and dihedrals were calculated with *X-PLOR* (Brünger, 1992). The overall stereochemical quality of the final models for PNP complexes was assessed using the program *PROCHECK* (Laskowski *et al.*, 1993) (Table 1). Atomic models were superposed using the program *LSQKAB* from *CCP*4 (Collaborative Computational Project, Number 4, 1994). The electrostatic potential surface of the ligands complexed with HsPNP was calculated using the program *GRASP* (Nicholls *et al.*, 1991) and the molecular-surface areas were calculated with *AREAIMOL* (Collaborative Computational Project, Number 4, 1994).

3. Results and discussion

3.1. Molecular replacement and crystallographic refinement

The standard procedure of molecular replacement using *AMoRe* (Navaza, 1994) was used to solve the structures. $2F_{obs} - F_{calc}$ omit maps were calculated. These maps showed electron density for the ligands in the complexes. The statistics of the molecular replacement and refinement are in Table 1. Fig. 2 shows the electron density for the active-site regions.

3.2. Overall description

The crystallographic structures of the complexes indicate that PNP is a homotrimer, with each subunit consisting of a distorted β-barrel structure flanked by seven α-helices. Human PNP is also a trimer in solution (de Azevedo, dos Santos *et al.*, 2003). The active site is located near the subunit–

Figure 3
Superposition of PNP apoenzyme with the PNP–guanine complex, showing the gate movement, which involves a helical transformation of residues 257–265 in the transition apoenzyme complex. Movements of the residues Tyr249, His257 and Lys265 and the position of ligand and sulfates can be observed. The figure was generated with the program *MOLMOL* (Koradi *et al.*, 1996).

subunit boundary, with seven different segments of one subunit and one segment of the other subunit contributing active-site residues.

The structures of human PNP show clear electron-density peaks for three sulfate groups; sulfate is present at a high concentration in the crystallization conditions. The first sulfate site is located near a glycine-rich loop (residues 32–37), which is the catalytic phosphate-binding site, and forms hydrogen bonds to Ser33, Arg84, His86 and Ser220. The residues Tyr88 and Ala116 interact *via* hydrogen bonds with the catalytic sulfate. The second sulfate-binding site lies near Gly35 and Gly36 and is exposed to the solvent; whether it is mechanistically significant or an artifact resulting from the high sulfate concentration used to grow the crystals is not known. The third identified sulfate group makes three hydrogen bonds, involving residues Gln144 and Arg148 from an adjacent subunit, corresponding to a regulatory site (de Azevedo, Canduri *et al.*, 2003).

3.3. Ligand-binding conformational changes

There is a conformational change in the PNP structures when ligands bind to the active site (Narayana *et al.*, 1997; de Azevedo *et al.*, 2003b; dos Santos *et al.*, 2003). The largest movement was observed for Ala263 in the present structure. Residues 241–260 act as a gate that opens during substrate binding. The r.m.s.d. in the C^{α} coordinates on superimposition of the HsPNP complexes on the PNP apoenzyme is 0.48 Å, disregarding the gate. The r.m.s.d. in the C^{α} coordinates (residues 5–285) is 1.24 Å upon superimposition of the complexes of HsPNP on the PNP apoenzyme. These are average values for the three PNP complexes. The gate is anchored near the central β-sheet at one end and near the C-terminal helix at the other end and is responsible for controlling access to the active site. The gate movement involves a helical transformation of residues 257–265 in the transition apoenzyme complex, with the largest movement observed for the His257 side chain, which partially occupies the purine subsite in the native enzyme. The superposition of this region of the HsPNP apoenzyme (PDB code 1m73; de Azevedo, Canduri *et al.*, 2003) with HsPNP complexed with guanine is shown in Fig. 3.

The analysis of these complexes indicates that the purine-binding site is composed of residues Glu201, Thr242 and Asn243. The ribose-binding site is mostly hydrophobic and is composed of several aromatic amino acids, including Tyr88, His86, His257, Ala116 and Met219. Remarkably, however, the hydrogen bond between the O2′ oxygen and the amide of Met219 seems to be the only enzymatic contact relevant to ribosyl-ring migration in the reaction-coordinate motion (Fedorov *et al.*, 2001).

3.4. Interactions with guanosine

Analysis of the hydrogen bonds between guanosine and PNP reveals eight hydrogen bonds: five hydrogen bonds with purine involving residues Glu201 and Asn243 and three with ribose involving residues His257, Tyr88 and Met219 (Fig. 4a).
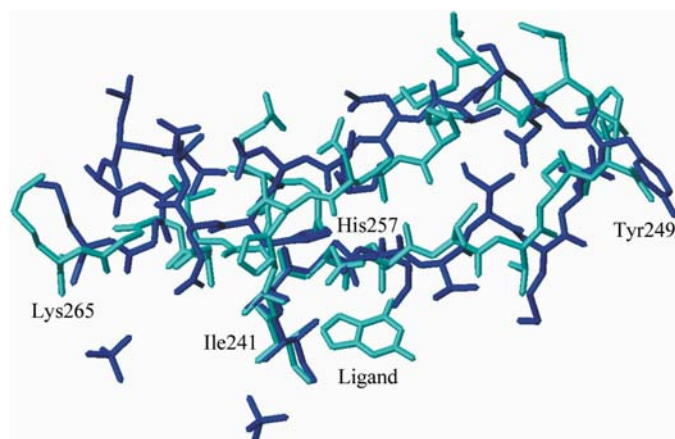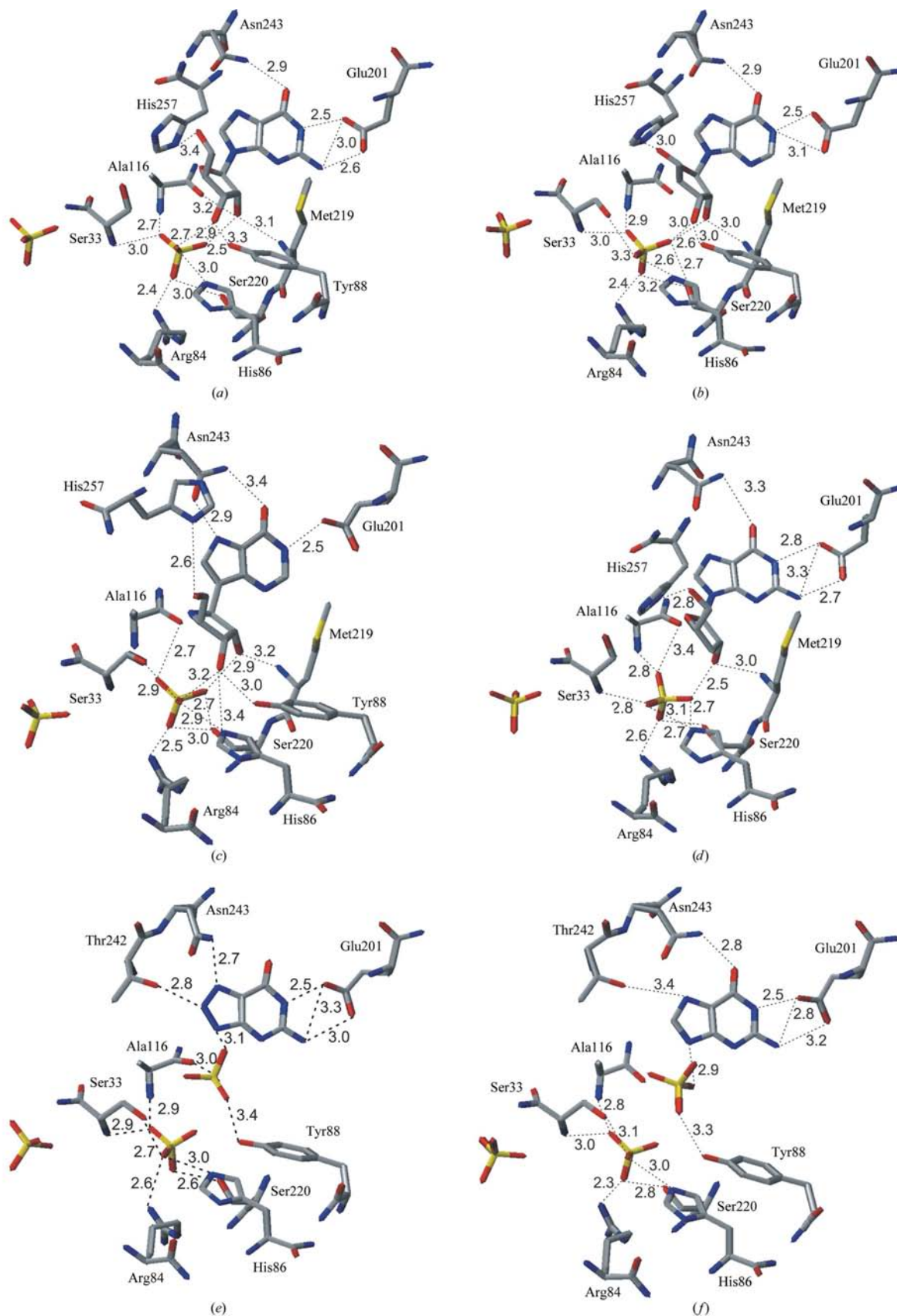
Figure 4
Binding site of human PNP. (*a*) HsPNP–guanosine, (*b*) HsPNP–inosine, (*c*) HsPNP–immucillin-H, (*d*) HsPNP–3′-deoxyguanosine, (*e*) HsPNP–8-azaguanine, (*f*) HsPNP–guanine.
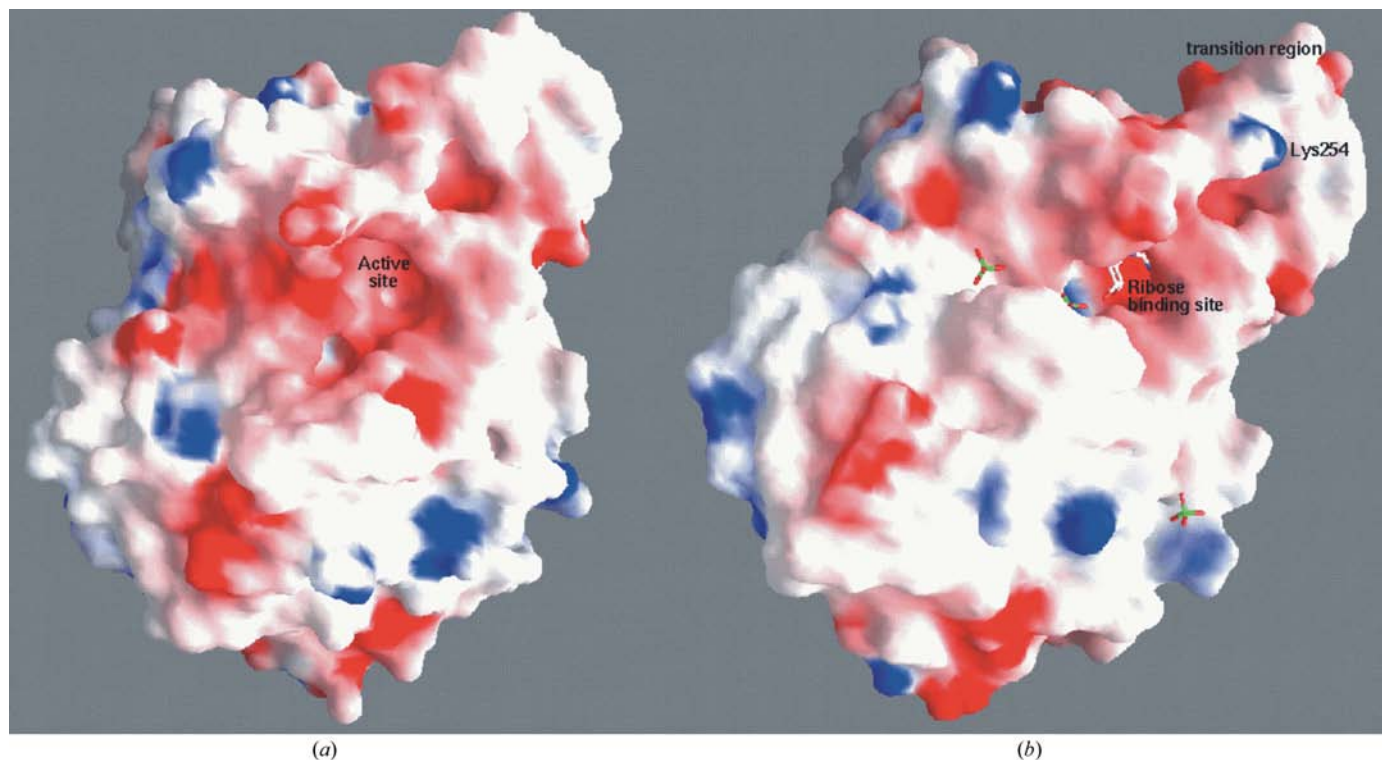
Figure 5
Electrostatic potential surface for the monomer of (*a*) HsPNP apoenzyme and (*b*) HsPNP in presence of the ligands, guanosine and sulfates, calculated with *GRASP* (Nicholls *et al.*, 1991) and shown from $-10kT$ (red) to $+10kT$ (blue). Uncharged regions are white. The molecular surface of the active site and the transition region of the gate are shown.

The PNP complexes indicated that PNP interacts with the ribose moiety through hydrogen bonds between the phenolic group of Tyr88 and O3′ and between the imidazole of His257 and O5′. The PNP–inosine and PNP–immucillin-H complexes show the same hydrogen-bonding pattern to the ribose moiety (Figs. 4*b* and 4*c*) and contact areas of 189 and 206 Å^2, respectively. The contact area between guanosine and HsPNP is 195 Å^2. These areas are close to the contact area observed in the HsPNP–dGuo complex.

3.5. Interactions with 3′-deoxyguanosine

Analysis of the hydrogen bonds between 3′-deoxyguanosine and PNP reveals four hydrogen bonds involving the residues Glu201 and Asn243 and one hydrogen bond to a water molecule in the active site. The interaction of the residues Met219 and His257 with the ribose is similar to guanosine. The 3′-deoxyguanosine shows a contact area with human PNP of 198 Å^2. 50% of this contact area is the purine-binding site. The analysis of the charge distribution of the binding pockets indicates the presence of some charge complementarity between substrate and enzyme, principally in the purine-binding site (Fig. 5). Fig. 2(*b*) shows the electron density in the active-site region for the complex.

3.6. Interactions with 8-azaguanine

Wierzchowski *et al.* (1996) analyzed the fluorescence emission properties of the neutral and ionic forms of the azapurine

nucleosides in an aqueous medium. The fluorescence properties of these compounds were used to determine the basic kinetic parameters for synthesis of 8-azapurine nucleosides by PNP from mammalian (calf spleen) and bacterial (*Escherichia coli*) sources. The most effective is 8-azaIno (K_i approximately 20 μ*M*), which is also the only one to inhibit phosphorolysis by the calf spleen enzyme (K_i approximately 40 μ*M*). The nature of this inhibition is apparently uncompetitive. Since the active site of bovine and human PNP is conserved, similar K_i values are expected for PNP from both sources. For the complex HsPNP–azaGua five hydrogen bonds were observed, involving residues Glu201, Thr242 and Asn243 (Fig. 4*e*). This interaction is similar to that observed in the PNP–Gua, PNP–Guo and PNP–dGuo complexes (Figs. 4*a*, 4*d* and 4*f*), with one additional hydrogen bond between Thr242 OG1 and the N8 of the purine.

The structure of HsPNP–azaGua showed the presence of a fourth sulfate group occupying the ribose-binding site, as observed in the PNP–Gua complex (de Azevedo *et al.*, 2003*a*). Fig. 2(*c*) shows the electron density of the active-site region. The 8-azaguanine ligand presents a contact area with HsPNP of 105 Å^2 and, considering the fourth sulfate that occupies the ribose site, the contact area is 199 Å^2, which is compatible with other ligands (guanosine, 195 Å^2 and 3′-deoxyguanosine, 198 Å^2). HsPNP–azaGua shows clear electron-density peaks for four sulfate groups. The fourth sulfate-binding site makes hydrogen bonds with residues Ser33 (3.2 Å), Tyr88 (3.4 Å) and Ala116 (3.0 Å) and it is close to 8-azaguanine, making

two hydrogen bonds to the nucleoside (3.0 and 3.1 Å; Fig. 4e).

4. Conclusions

Analysis of the present human PNP structures strongly indicates induced conformational changes in the protein arising from ligand binding. There is a large movement of residues 241–260 in the PNP structure in the presence of ligands. The loop 241–260 is flexible in the native structure and functions as a swinging gate to allow the substrate in and out of the active site (Narayana *et al.*, 1997; Figs. 3 and 5). Residues 257–265 form a helix, changing the position of the side chain of the residues on ligand binding. Analysis of the complexes indicates that Glu201, Thr242 and Asn243 are the main residues involved in binding of the purine ring and occupy approximately the same position in all the complexes. The K_m values for the affinity of human PNP for guanosine and inosine have been previously determined and are 12 and 45 µM, respectively (Bzowska *et al.*, 2000). Analysis of the interaction between these ligands and HsPNP indicates a higher number of intermolecular hydrogen bonds (eight) between HsPNP and guanosine (Fig. 4a), which correlates with the lower K_m value observed for guanosine compared with inosine, which presents six intermolecular hydrogen bonds.

References

Azevedo, W. F. de, Canduri, F., dos Santos, D. M., Pereira, J. H., Dias, M. V. B., Silva, R. G., Mendes, M. A., Basso, L. A., Palma, M. S. & Santos, D. S. (2003a). *Biochem. Biophys. Res. Commun.* **312**, 767–772.

Azevedo, W. F. de, Canduri F., dos Santos, D. M., Pereira, J. H., Dias, M. V. B., Silva, R. G., Mendes, M. A., Basso, L. A., Palma, M. S. & Santos, D. S. (2003b). *Biochem. Biophys. Res. Commun.* **309**, 917–922.

Azevedo, W. F. de Jr, Canduri, F., dos Santos, D. M., Silva, R. G., Oliveira, J. S., Carvalho, L. P. S., Basso, L. A., Mendes, M. A., Palma, M. S. & Santos, D. S. (2003). *Biochem. Biophys. Res. Commun.* **308**, 545–552.

Azevedo, W. F. de Jr, dos Santos, G. C., dos Santos, D. M., Olivieri, J. R., Canduri, F., Silva, R. G., Basso, L. A., Renard, G., da Fonseca, I. O., Mendes, M. A., Palma, M. S. & Santos, D. S. (2003). *Biochem. Biophys. Res. Commun.* **309**, 923–928.

Bantia, S., Ananth, S. L., Parker, C. D., Horn, L. L. & Upshaw, R. (2003). *Int. Immunopharmacol.* **3**, 879–887.

Bantia, S., Miller, P. J., Parker, C. D., Ananth, S. L., Horn, L. L., Kilpatrick, J. M., Morris, P. E., Hutchison, T. L., Montgomery, J. A. & Sandhu, J. S. (2001). *Int. Immunopharmacol.* **1**, 1199–1210.

Brünger, A. T. (1992). *X-PLOR Version 3.1. A System for Crystallography and NMR*. New Haven: Yale University Press.

Bzowska, A., Kulikowska, E. & Shugar, D. (2000). *Pharmacol. Ther.* **88**, 349–425.

Canduri, F., dos Santos, D. M., Silva, R. G., Mendes, M. A., Basso, L. A., Palma, M. S., de Azevedo, W. F. & Santos, D. S. (2004). *Biochem. Biophys. Res. Commun.* **313**, 907–914.

Canduri, F., Fadel, V., Basso, L. A., Palma, M. S., Santos, D. S. & de Azevedo, W. F. Jr (2005). *Biochem. Biophys. Res. Commun.* **327**, 646–649.

Canduri, F., Fadel, V., Dias, M. V. B., Basso, L. A., Palma, M. S., Santos, D. S. & de Azevedo, W. F. Jr (2005). *Biochem. Biophys. Res. Commun.* **326**, 335–338.

Cohen, A., Doyle, D., Martin, D. W. Jr & Ammann, A. J. (1976). *N. Engl. J. Med.* **295**, 1449–1454.

Collaborative Computational Project, Number 4 (1994). *Acta Cryst.* D**50**, 760–763.

Cook, W. J., Ealick, S. E., Bugg, C. E., Stoeckler, J. D. & Parks, R. E. Jr (1981). *J. Biol. Chem.* **256**, 4079–4080.

Ealick, S. E., Babu, Y. D., Bugg, C. E., Erion, M. D., Guida, W. C., Montgomery, J. A. & Secrist, J. A. III (1991). *Proc. Natl Acad. Sci. USA*, **88**, 11540–11544.

Ealick, S. E., Rule, S. A., Carter, D. C., Greenhough, T. J., Babu, Y. S., Cook, W. J., Habash, J., Helliwell, J. R., Stoeckler, J. D., Parks, R. E. Jr, Chen, S.-F. & Bugg, C. E. (1990). *J. Biol. Chem.* **265**, 1812–1820.

Erion, M. D., Stoeckler, J. D., Guida, W. C., Walter, R. L. & Ealick, S. E. (1997). *Biochemistry*, **36**, 11735–11748.

Fedorov, A., Shi, W., Kicska, G., Fedorov, E., Tyler, P. C., Furneaux, R. H., Hanson, J. C., Gainsford, G. J., Larese, J. Z., Schramm, V. L. & Almo, S. C. (2001). *Biochemistry*, **40**, 853–860.

Hershfield, B. S. & Mitchell, B. S. (2001). *The Metabolic Basis of Inherited Disease*, 8th ed., edited by C. R. Scriber, A. L. Beaudet, W. S. Sly & D. Valle, pp. 2585–2624. New York: McGraw–Hill.

Kim, B. K., Cha, S. & Parks, R. E. Jr (1968). *J. Biol. Chem.* **243**, 1771–1776.

Kline, P. C. & Schramm, V. L. (1993). *Biochemistry*, **32**, 13212–13219.

Kline, P. C. & Schramm, V. L. (1995). *Biochemistry*, **34**, 1153–1162.

Koradi, R., Billeter, M. & Wuthrich, K. (1996). *J. Mol. Graph.* **14**, 51–55.

Krenitsky, T. A., Tuttle, J. V., Koszalka, G. W., Chen, I. S., Beacham, L. M. III, Rideout, J. L. & Elion, G. B. (1976). *J. Biol. Chem.* **251**, 4055–4061.

Laskowski, R. A., MacArthur, M. W., Moss, D. S. & Thornton, J. M. (1993). *J. Appl. Cryst.* **26**, 283–291.

McRee, D. E. (1999). *J. Struct. Biol.* **125**, 156–165.

Narayana, S. V., Bugg, C. E. & Ealick, S. E. (1997). *Acta Cryst.* D**53**, 131–142.

Navaza, J. (1994). *Acta Cryst.* A**50**, 157–163.

Nicholls, A., Sharp, K. & Honig, B. (1991). *Proteins Struct. Funct. Genet.* **11**, 281–296.

Northrop, D. B. (1975). *Biochemistry*, **14**, 2644–2651.

Santos, D. M. dos, Canduri, F., Pereira, J. H., Dias, M. V. B., Silva, R. G., Mendes, M. A., Palma, M. S., Basso, L. A., de Azevedo, W. F. & Santos, D. S. (2003). *Biochem. Biophys. Res. Commun.* **308**, 553–559.

Schramm, V. L. (2002). *Biochim. Biophys. Acta*, **1587**, 107–117.

Schramm, V. L. (2003). *Nucleic Acids Res. Suppl.* **3**, 107–108.

Silva, R. G., Carvalho, L. P., Oliveira, J. S., Pinto, C. A., Mendes, M. A., Palma, M. S., Basso, L. A. & Santos, D. S. (2003). *Protein Expr. Purif.* **27**, 158–164.

Simmonds, H. A., Fairbanks, L. D., Morris, G. S., Morgan, G., Watson, A. R., Timms, P. & Singh, B. (1987). *Arch. Dis. Child.* **62**, 385–391.

Stoeckler, J. D., Cambor, C. & Parks, R. E. Jr (1980). *Biochemistry*, **19**, 102–107.

Ullman, B., Gudas, L. J., Clift, S. M. & Martin, D. W. Jr (1979). *Proc. Natl Acad. Sci. USA*, **76**, 1074–1078.

Wierzchowski, J., Wielgus-Kutrowska, B. & Shugar, D. (1996). *Biochim. Biophys. Acta*, **1290**, 9–17.